A&A 629, A6 (2019)
https://doi.org/10.1051/0004-6361/201935603

Astronomy & Astrophysics

ALMA view of the $^{12}C/^{13}C$ isotopic ratio in starburst galaxies*

X. D. Tang[1,2,3], C. Henkel[3,4,1], K. M. Menten[3], Y. Gong[3], S. Martín[5,6], S. Mühle[7], S. Aalto[8], S. Muller[8], S. García-Burillo[9], S. Levshakov[10], R. Aladro[3], M. Spaans[11], S. Viti[12], H. M. Asiri[4], Y. P. Ao[13], J. S. Zhang[14], X. W. Zheng[15], J. Esimbek[1,2], and J. J. Zhou[1,2]

[1] Xinjiang Astronomical Observatory, Chinese Academy of Sciences, 830011 Urumqi, PR China
e-mail: tangxindi@xao.ac.cn
[2] Key Laboratory of Radio Astronomy, Chinese Academy of Sciences, 830011 Urumqi, PR China
[3] Max-Planck-Institut für Radioastronomie, Auf dem Hügel 69, 53121 Bonn, Germany
e-mail: chenkel@mpifr-bonn.mpg.de
[4] Astronomy Department, King Abdulaziz University, PO Box 80203, 21589 Jeddah, Saudi Arabia
[5] European Southern Observatory, Alonso de Córdova 3107, Vitacura Casilla, 763 0355 Santiago, Chile
[6] Joint ALMA Observatory, Alonso de Córdova 3107, Vitacura Casilla, 763 0355 Santiago, Chile
[7] Argelander Institut für Astronomie, Universität Bonn, Auf dem Hügel 71, 53121 Bonn, Germany
[8] Department of Earth and Space Sciences, Chalmers University of Technology, Onsala Observatory, 43992 Onsala, Sweden
[9] Observatorio de Madrid, OAN-IGN, Alfonso XII, 3, 28014 Madrid, Spain
[10] Ioffe Physical-Technical Institute, Polytekhnicheskaya Str. 26, 194021 St. Petersburg, Russia
[11] Kapteyn Astronomical Institute, University of Groningen, PO Box 800, 9700 AV Groningen, The Netherlands
[12] Department of Physics and Astronomy, UCL, Gower St., London WC1E 6BT, UK
[13] Purple Mountain Observatory, Chinese Academy of Sciences, Nanjing 210008, PR China
[14] Center for Astrophysics, Guangzhou University, 510006 Guangzhou, PR China
[15] School of Astronomy and Space Science, Nanjing University, 210093 Nanjing, PR China

Received 3 April 2019 / Accepted 15 June 2019

ABSTRACT

We derive molecular-gas-phase $^{12}C/^{13}C$ isotope ratios for the central few hundred parsecs of the three nearby starburst galaxies NGC 253, NGC 1068, and NGC 4945 making use of the $\lambda \sim 3$ mm ^{12}CN and ^{13}CN $N = 1$–0 lines in the ALMA Band 3. The $^{12}C/^{13}C$ isotopic ratios derived from the ratios of these lines range from 30 to 67 with an average of 41.6 ± 0.2 in NGC 253, from 24 to 62 with an average of 38.3 ± 0.4 in NGC 1068, and from 6 to 44 with an average of 16.9 ± 0.3 in NGC 4945. The highest $^{12}C/^{13}C$ isotopic ratios are determined in some of the outskirts of the nuclear regions of the three starburst galaxies. The lowest ratios are associated with the northeastern and southwestern molecular peaks of NGC 253, the northeastern and southwestern edge of the mapped region in NGC 1068, and the very center of NGC 4945. In the case of NGC 1068, the measured ratios suggest inflow from the outer part of NGC 1068 into the circum-nuclear disk through both the halo and the bar. Low $^{12}C/^{13}C$ isotopic ratios in the central regions of these starburst galaxies indicate the presence of highly processed material.

Key words. galaxies: abundances – galaxies: starburst – galaxies: nuclei – galaxies: ISM – radio lines: ISM

1. Introduction

Even though interstellar carbon isotope ratios are locally understood (e.g., Wilson & Rood 1994; Henkel et al. 1994a; Wilson 1999), in extragalactic space beyond the Magellanic Clouds they are almost unexplored. We lack information on objects outside the Local Group of galaxies tracing environments that drastically differ from those in the Milky Way and the Large Magellanic Cloud (LMC). We do not know whether our Galaxy is typical for its class of objects or whether its isotopic properties are exceptional. What would the latter imply? Moreover, will we see strong variations in isotopic ratios when observing nearby galaxies with high angular resolution?

In the past, observational data have been mostly obtained for the Galaxy and the Magellanic Clouds (e.g., Wouterloot & Brand 1996; Wouterloot et al. 2008; Wang et al. 2009). A surprising result is that the metal-poor outer Galaxy is not merely providing a "bridge" between the solar neighborhood and the even more metal-poor LMC. This is explained by the different age of the bulk of the stellar populations of the outer Galaxy and the LMC and can be exemplified by the $^{12}C/^{13}C$ and $^{18}O/^{17}O$ ratios, which are both a measure of "primary" versus "secondary" nuclear processing. While ^{12}C and ^{18}O are produced on rapid timescales primarily via He burning in massive stars, ^{13}C and ^{17}O are predominantly synthesized via CNO processing of ^{12}C and ^{16}O seeds from earlier stellar generations. The latter occurs on a slower timescale during the red-giant phase in low- and intermediate-mass stars or novae (e.g., Wilson & Rood 1994; Henkel et al. 1994a,b).

Molecular spectroscopy is fundamentally important to constrain stellar nucleosynthesis and the chemical evolution of galaxies. Atomic spectroscopy of stellar or interstellar gas does not allow us to discriminate between different isotopic species. However, isotopic abundances are readily obtained by

* A copy of the reduced datacubes is available at the CDS via anonymous ftp to cdsarc.u-strasbg.fr (130.79.128.5) or via http://cdsarc.u-strasbg.fr/viz-bin/qcat?J/A+A/629/A6

spectroscopy of molecular isotopologs (Henkel et al. 1994a). Locally, emphasizing carbon, observational constraints show very high molecular-gas-phase $^{12}C/^{13}C$ ratios ($^{12}C/^{13}C$ given here and elsewhere represent the molecular gas) from molecular spectroscopy in the outer Galaxy (>100), high ratios in the local interstellar medium (ISM; ~70), lower ones in the inner galactic disk and LMC (~50), and a smaller value (~20–25) in the galactic center region (e.g., Güsten et al. 1985; Wilson & Rood 1994; Henkel et al. 1994a; Wouterloot & Brand 1996; Wilson 1999; Wang et al. 2009). The solar system ratio (~89; Wilson & Rood 1994; Henkel et al. 1994a) can be interpreted to represent conditions at a time when the local disk was 4.6×10^9 yr younger than today. Within the framework of "biased infall" (e.g., Chiappini et al. 2001) the galactic disk is slowly formed from the inside out, causing gradients in the abundances across the disk. The stellar ^{13}C ejecta, reaching the ISM with a time delay, are less dominant in the young stellar disk of the outer Galaxy than in the inner Galaxy and in the older stellar body of the LMC (for the LMC, see Hodge 1989). The solar-system ratio, referring to a younger disk with less ^{13}C, is consequently higher than that measured in the present local ISM.

While the ^{13}C-bearing molecular species can be safely assumed to be optically thin (with the possible exception of ^{13}CO), a basic problem is the optical depth of the ^{12}C bearing species (e.g., HCN, HCO^+; Nguyen et al. 1992; Wild et al. 1992; Henkel et al. 1993; Gao & Solomon 2004; Jiang et al. 2011; Wang et al. 2014; Davis 2014; Jiménez-Donaire et al. 2017). Beam filling factors, $\tau(^{12}CX)$, are in most cases unknown when it comes to extragalactic sources. With this in mind, a useful tracer should possess the following properties:

- The tracer must be abundant, showing strong lines, to allow us to also detect the rare species, but not be so strong (i.e., opacity ~1) as to cause optical thickness problems.
- A useful check of the opacity should be provided by transitions exhibiting fine and hyperfine structure (fs and hfs, respectively). In such cases the splitting should be wide enough for the different components to be separated for a line emission with a width of several hundred kilometers per second, commonly encountered in external galaxies.
- The components should show, in the optically thin limit, relative intensities as predicted by local thermodynamical equilibrium (LTE). Line ratios deviating from these values can then be used for optical depth estimates.
- The tracer must be well understood theoretically and observationally; the former in terms of its physical and chemical properties related to photodissociation and fractionation, the latter by a systematic survey of $^{12}C/^{13}C$ ratios in galactic star-forming regions.
- Finally, there should be no blend with any other potential strong line of another species.

Presently, there is only one molecule matching all these conditions, the cyanide radical (CN). The molecule C_2H may come close but a systematic galactic survey based on this molecule has not yet been conducted. Previous observations show that CN is widespread in galactic molecular clouds (e.g., Rodríguez-Franco et al. 1998; Han et al. 2015; Gratier et al. 2017; Watanabe et al. 2017; Yamagishi et al. 2018) and a variety of other objects, including the circumstellar envelopes of evolved stars (e.g., Bachiller et al. 1997; Savage et al. 2002; Milam et al. 2005, 2009; Hily-Blant et al. 2008; Adande & Ziurys 2012). It was detected for the first time in extragalactic sources by Henkel et al. (1988), and exhibits strong lines, allowing it to be easily detected outside the Galaxy. (e.g., Henkel et al. 1988, 1990, 1991, 1993, 1994b, 1998, 2014; Aalto et al. 2002, 2007; Wang et al. 2004, 2009; Fuente et al. 2005; Pérez-Beaupuits et al. 2007, 2009; García-Burillo et al. 2010; Chung et al. 2011; Martín et al. 2011; Aladro et al. 2013, 2015; Meier et al. 2014, 2015; Sakamoto et al. 2014; Watanabe et al. 2014; Ginard et al. 2015; Nakajima et al. 2015, 2018; Saito et al. 2015; König et al. 2016; Qiu et al. 2018; Wilson 2018).

Cyanide spectra are complex. Each CN rotational energy level with $N > 0$ is split into a doublet by spin-rotation interaction. Because of the spin of the nitrogen nucleus ($I_1 = 1$), each of these components is further split into a triplet of states. The ^{13}CN spectrum is further complicated by the spin of the ^{13}C nucleus ($I_2 = 1/2$). All this results in a very complex hfs splitting of the rotational lines. Numerically, it has been shown that carbon ratios resulting from CN measurements should not be affected by isotope selective photodissociation or chemical fractionation (Langer et al. 1984; Roueff et al. 2015). Observationally, this has been confirmed by Savage et al. (2002) and Milam et al. (2005).

Previous observations of CN in the Milky Way indicate a $^{12}C/^{13}C$ isotope ratio gradient with galactocentric distance (Savage et al. 2002; Milam et al. 2005), which agrees rather well with the gradient derived from measurements of CO and H_2CO (e.g., Henkel et al. 1980, 1982, 1983, 1985, 1994a; Langer & Penzias 1990, 1993; Wilson & Rood 1994; Giannetti et al. 2014; Yan et al. 2019). This suggests that the $^{12}C/^{13}C$ isotope ratios obtained from CN are an excellent indicator of galactic chemical evolution (Milam et al. 2005). This is even more true for extragalactic targets, since CO and the millimeter-wave lines of H_2CO do not allow for direct determinations of optical depths of the main species, while the centimeter-wave lines of $H_2^{13}CO$ are extremely weak.

So far, few $^{12}C/^{13}C$ isotope ratio determinations of extragalactic targets have been performed. In this study, we therefore carried out observations of three nearby starburst galaxies, NGC 253, NGC 1068, and NGC 4945. In Sects. 2 and 3, we introduce our targets, observations of CN, data reduction, and describe the main results. The resulting carbon isotope ratio derived from CN is then discussed in Sect. 4. Our main conclusions are summarized in Sect. 5.

2. Targets, observations, and data reduction

2.1. Targets

The three objects we selected, namely NGC 253, NGC 1068, and NGC 4945, are prominent nearby starburst galaxies, exhibiting particularly strong molecular lines (e.g., Martín et al. 2006; Chou et al. 2007; García-Burillo et al. 2010, 2014, 2016, 2017; Aladro et al. 2013; Meier et al. 2015; Henkel et al. 2018). The choice of the galaxies was made to have three of the strongest extragalactic line emitters and to cover a certain range of starbursts, that is, the transition from "moderate starbursts" (NGC 253 and NGC 4945) to more luminous infrared galaxies (LIRGs; NGC 1068). Single-dish spectral line surveys have been performed for all our selected starburst galaxies in the 3 mm band (e.g., Henkel et al. 1990, 1994b; Wang et al. 2004; Aladro et al. 2013, 2015; Nakajima et al. 2018). The $^{12}C/^{13}C$ isotope ratio is ~40 estimated from CN and CS (Henkel & Mauersberger 1993; Henkel et al. 1993, 2014), but >81 obtained from C_2H (Martín et al. 2010), in the starburst galaxy NGC 253. Interferometric measurements of $^{12}C^{18}O/^{13}C^{18}O$ in NGC 253 indicate a low value of ~21 (Martín et al. 2019). This same ratio is ~50 obtained from CN in NGC 1068 (Aladro et al. 2013) and a value of 40–50 was reported in NGC 4945 (Henkel & Mauersberger 1993; Henkel et al. 1994b; Wang et al. 2004). Toward M 82 and

Table 1. Main properties of the galaxies and observational parameters.

Source	RA(J2000) h m s	Dec(J2000) ° ′ ″	Distance [a] Mpc	Beam size "×"	Beam size pc × pc	Position angle °	Type [a]
NGC 253	00:47:33.14	–25:17:17.5	3.9	3.6 × 1.7	~68 × 32	82	SAB(s)c; Starburst
NGC 1068	02:42:40.70	–00:00:48.0	14.4	4.5 × 2.2	~314 × 154	75	(R)SA(rs)b; AGN+Starburst
NGC 4945	13:05:27.50	–49:28:06.0	3.8	3.6 × 2.3	~66 × 42	81	SB(s)cd; AGN+Starburst

Notes. [a]Distances and type were taken from the NASA/IPAC Extragalactic Database (NED).

IC 342, Henkel et al. (1998) found $^{12}C/^{13}C > 40$ and >30 from CN. For Arp 220 and Mrk 231, it appears to be 100 from CO and OH (González-Alfonso et al. 2012; Henkel et al. 2014), and for the Cloverleaf QSO it may be >100 from CO (Henkel et al. 2010). These determined values indicate a trend matching qualitative expectations of decreasing $^{12}C/^{13}C$ values with time and metallicity (Henkel et al. 2014). However, all classes of sources targeted so far only encompass one or two objects.

Below follows a brief description of the selected targets. NGC 253, the Sculptor galaxy, an almost edge-on barred spiral (Pence 1981; Puche et al. 1991), is one of the most prolific infrared and molecular lighthouses of the entire extragalactic sky. At a distance of ~3.9 Mpc (e.g., Mouhcine et al. 2005; Rekola et al. 2005), it is a prime example of a galaxy with a nuclear starburst devoid of an active galactic nucleus (AGN; e.g., Ulvestad & Antonucci 1997; Henkel et al. 2004). Because of the exceptional strength of its molecular lines, NGC 253 was selected as the target of choice for the first unbiased molecular line survey of an extragalactic source (Martín et al. 2006). It is therefore a highly suitable target for this study.

NGC 1068, a local LIRG and a prototypical Seyfert 2 galaxy with a starburst at a distance of ~14.4 Mpc (Bland-Hawthorn et al. 1997), is one of the best extragalactic targets for studying the physical and chemical properties of the ISM in the vicinity of an AGN. Numerous molecular line observations have targeted the circumnuclear molecular ring of NGC 1068 and the effect of nuclear activity on its ISM (e.g., Schinnerer et al. 2000; Usero et al. 2004; García-Burillo et al. 2010, 2014, 2016, 2017; Krips et al. 2011; Aladro et al. 2013; Viti et al. 2014; Wang et al. 2014; Qiu et al. 2018). Water maser emission has been observed forming an edge-on disk in the circumnuclear environment of NGC 1068 (e.g., Greenhill et al. 1996; Gallimore et al. 1996, 1997, 2001).

NGC 4945, at a distance of ~3.8 Mpc (e.g., Karachentsev et al. 2007; Mould & Sakai 2008), has an active Seyfert 2 nucleus and is, like NGC 253, an almost edge-on spiral galaxy. Its central region is known to show a rich molecular spectrum hosting not only a nuclear starburst but also an AGN (e.g., Marconi et al. 2000; Yaqoob 2012). Past molecular single-dish and interferometric observational studies exist for CO, CS, CN, HCN, HNC, HCO^+, CH_3OH, and H_2CO (e.g., Henkel et al. 1990, 1994b, 2018; Dahlem et al. 1993; Mauersberger et al. 1996; Curran et al. 2001; Wang et al. 2004; Chou et al. 2007; Hitschfeld et al. 2008; Green et al. 2016; McCarthy et al. 2018). Water megamaser emission has been observed in the nucleus of NGC 4945 (Greenhill et al. 1997).

2.2. Observations

Our observations were carried out from 2014 December to 2015 January with the Atacama Large Millimeter/submillimeter Array (ALMA) in Band 3 (Project: 2013.1.01151.S). During the observations, 36–40 12 m antennas were employed in a compact configuration with baselines ranging from 15 to 349 m. For each source, the observations took about 30 min and 1 h for ^{12}CN and ^{13}CN, respectively. The CN $N = 1–0$ transition consists of nine hyperfine components blended into two groups, with the stronger group representing the $J = 3/2–1/2$ transitions and the weaker group the $J = 1/2–1/2$ transitions. The ^{12}CN $N = 1–0$ ($J = 1/2–1/2$ and $3/2–1/2$) and ^{13}CN $N = 1–0$ ($J = 1/2–1/2$ and $3/2–1/2$) transitions have intensity weighted rest frequencies of 113.191, 113.491, 108.658, and 108.780 GHz, respectively, when LTE line ratios and optically thin emission are adopted. On each, the ^{12}CN and the ^{13}CN line, a spectral window was centered, with a bandwidth of 1875 MHz and a frequency resolution of 7812.5 kHz, corresponding to a channel width of ~21 km s^{-1}. Basic observational parameters as well as phase center coordinates are listed in Table 1. The ^{12}CN data of NGC 253 were not part of our project. Instead, Meier et al. (2015) observed NGC 253 in ^{12}CN $N = 1–0$ with ALMA Band 3 (Project: 2011.0.00172.S). Quality and in particular beam sizes of these data match our ALMA observations well. ^{12}CN $N = 1–0$ data of NGC 253 are therefore taken from Meier et al. (2015) in this work. The observed spectra toward the central positions of NGC 253, NGC 1068, and NGC 4945 are shown in Fig. 1.

2.3. Data reduction

The data were calibrated and imaged using the CASA[1] 4.2 version pipeline (McMullin et al. 2007). Our ^{13}CN data reduction for NGC 253 (see Table 1) follows that performed for the ^{12}CN data set (beam size ~3.8″ × 2.7″ and position angle –31°) by Meier et al. (2015). The spectral line images were analyzed using GILDAS[2]. Typical rms noise levels in the ^{12}CN and ^{13}CN velocity-integrated intensity images are 1–2 and 0.3–0.7 mJy beam^{-1} for NGC 253, 1–2 and 0.4–0.7 mJy beam^{-1} for NGC 1068, and 2–4 and 0.4–0.9 mJy beam^{-1} for NGC 4945, respectively.

2.4. Spatial filtering

As mentioned in Sect. 2.1, the CN $N = 1–0$ transitions have previously been observed using the 15 m SEST (beam size ~44″), 30 m IRAM (beam size ~22″), and 45 m NRO (beam size ~15″) telescopes toward NGC 253, NGC 1068, and NGC 4945 (Henkel et al. 1990, 1994b, 2014; Wang et al. 2004; Aladro et al. 2013, 2015; Nakajima et al. 2018). From these observations $^{12}C/^{13}C$ isotope ratios of 40±10, ~50, and 40–50, respectively, were determined. One should note that the ^{13}CN $N = 1–0$ features observed with the 30 m IRAM telescope by Aladro et al. (2013) are weak and show low signal-to-noise ratios (S/Ns). Both ^{12}CN

[1] https://casa.nrao.edu
[2] http://www.iram.fr/IRAMFR/GILDAS

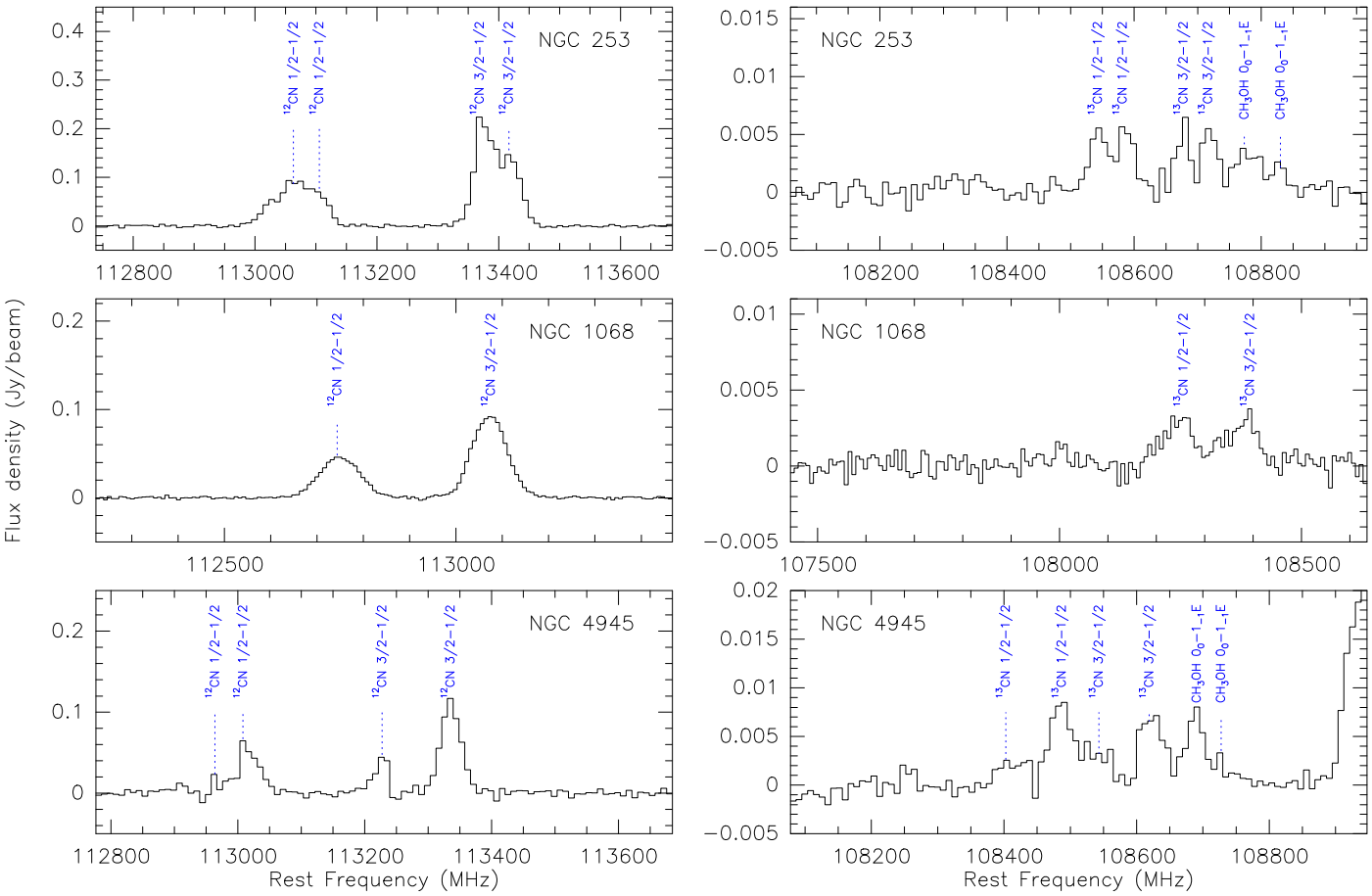

Fig. 1. ^{12}CN $N = 1$–0 (*left*) and ^{13}CN $N = 1$–0 (*right*) spectra toward NGC 253 (*top*), NGC 1068 (*middle*), and NGC 4945 (*bottom*) obtained with ALMA toward the central position (see Table 1).

and ^{13}CN $N = 1$–0 lines of NGC 1068 were detected with slightly higher S/Ns with the 45 m NRO telescope (Nakajima et al. 2018). A ^{12}C/^{13}C isotope ratio of ~40 in NGC 1068 was calculated from the integrated intensity ratio of $I(^{12}\mathrm{CN})/I(^{13}\mathrm{CN})$ by Nakajima et al. following our method mentioned in Sect. 3.4. For NGC 4945, the ^{13}CN $N = 1$–0 transition was not detected by Wang et al. (2004).

Due to spatial filtering, the missing flux, that is flux of large-scale structures not sampled by the interferometer, may affect ^{12}CN/^{13}CN line ratios. To evaluate the missing flux we reconstruct our ALMA data with beams of ~22″ (IRAM 30 m; Henkel et al. 2014; Aladro et al. 2015), ~15″ (NRO 45 m; Nakajima et al. 2018), and ~44″ (SEST 15 m; Wang et al. 2004) for NGC 253, NGC 1068, and NGC 4945, respectively. We find that ~89% and ~86% of the ^{12}CN and ^{13}CN integrated flux observed by single-dish telescopes is recovered for NGC 253 by our ALMA data, respectively. Only ~30% and ~53% of the ^{12}CN and ^{13}CN single-dish integrated flux of NGC 1068 is recovered, respectively. However, as mentioned above, the ^{13}CN $N = 1$–0 features observed with the 45 m NRO telescope (Nakajima et al. 2018) are weak and show large uncertainties. For NGC 4945, ~63% of the ^{12}CN single-dish integrated flux is recovered. We do not evaluate the missing flux of ^{13}CN in NGC 4945 because (as already mentioned) the ^{13}CN $N = 1$–0 transition was not detected with the 15 m SEST (Wang et al. 2004). In their Table 2, Wang et al. (2004) provide an upper limit (3 sigma) to the ^{13}CN $N = 1$–0 line intensity, so at least ~40% is recovered by our ALMA data. Based on similar missing flux of our ^{12}CN and ^{13}CN data in NGC 253 and NGC 1068, we note that ^{13}CN $N = 1$–0 is likely showing a less extended morphology (see Sect. 3.1) only because it is more rapidly reaching intensities below the detection threshold outside the line peaks. Therefore, our ^{13}CN data may cover a single-dish integrated flux fraction which is similar to that of ^{12}CN in NGC 4945. With similar missing flux levels related to our ^{12}CN and ^{13}CN data in NGC 253 and NGC 1068, which is based on a comparison of our interferometric measurements with previously published single-dish observations, missing flux appears to affect ^{12}CN/^{13}CN line ratios in NGC 253, NGC 1068, and NGC 4945 only weakly.

There may be line blending with the CH_3OH (0_0–1_{-1} E) transition at 108.894 GHz, 114 MHz (~300 km s^{-1}) away from the group of ^{13}CN ($N = 1$–0; $J = 3/2$–$1/2$) lines centered at 108.780 GHz (see Sect. 2 and Fig. 1). However, CH_3OH can be clearly identified in most locations of NGC 253 and NGC 4945, which indicates that the $I(^{12}\mathrm{CN})/I(^{13}\mathrm{CN})$ ratios are at most only weakly affected by CH_3OH in these two galaxies. For NGC 1068, the typical line widths of ^{13}CN are broader (~170 km s^{-1}) and CH_3OH cannot be identified in most locations. This could indicate that the $I(^{12}\mathrm{CN})/I(^{13}\mathrm{CN})$ ratio may be underestimated from our ALMA data in NGC 1068. The slightly less extended ^{13}CN distributions also addressed in Sect. 3.1 when compared to ^{12}CN may merely indicate that the minimum detectable molecular H_2 column density is higher than in the case of ^{12}CN with its higher fractional abundance (see also Sect. 3.3).

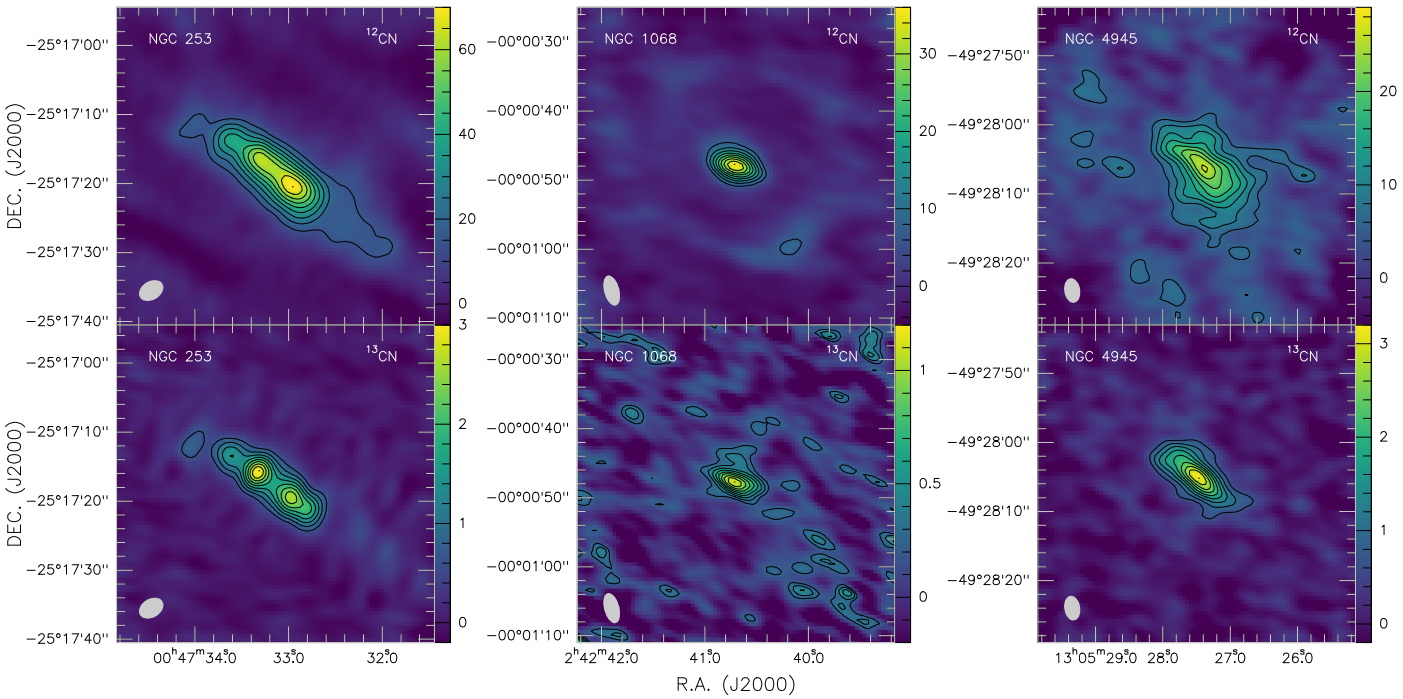

Fig. 2. Integrated intensity maps (color bars in units of Jy beam^{-1} km s^{-1}) of ^{12}CN ($I(^{12}\mathrm{CN}\ J=1/2–1/2)+I(^{12}\mathrm{CN}\ J=3/2–1/2)$) and ^{13}CN ($I(^{13}\mathrm{CN}\ J=1/2–1/2)+I(^{13}\mathrm{CN}\ J=3/2–1/2)$) of NGC 253 (^{12}CN and ^{13}CN integrated frequency range: 112.960–113.491 and 108.526–108.744 GHz; *left*), NGC 1068 (^{12}CN and ^{13}CN integrated frequency range: 112.641–113.169 and 108.170–108.459 GHz; *middle*), and NGC 4945 (^{12}CN and ^{13}CN integrated frequency range: 112.809–113.377 and 108.363–108.653 GHz; *right*). The contour levels are from 20% to 100% with steps of 10% for ^{12}CN and ^{13}CN of the peak intensity. The ^{12}CN peak intensities are 71.9, 35.8, and 26.4 Jy beam^{-1} km s^{-1}, and the ^{13}CN peak intensities are 3.0, 1.1, and 3.2 Jy beam^{-1} km s^{-1} in NGC 253, NGC 1068, and NGC 4945, respectively. For the ^{12}CN map of NGC 253, see also Meier et al. (2015). The pixel size of each image is 0.3″ × 0.3″. The synthesized beam of each image is shown in the *lower left corner*.

3. Results

3.1. Distribution of ^{12}CN and ^{13}CN

The integrated intensity distributions of ^{12}CN and ^{13}CN in NGC 253, NGC 1068, and NGC 4945 are shown in Fig. 2. In all three galaxies ^{12}CN shows extended distributions, in agreement with previous observations of ^{12}CN in galaxies (e.g., Henkel et al. 1988; García-Burillo et al. 2010; Meier et al. 2014; Sakamoto et al. 2014; Ginard et al. 2015; Nakajima et al. 2015; Saito et al. 2015; Wilson 2018). This is also consistent with previous observational results for other gas tracers such as for example ^{13}CO, C^{18}O, CS, HCN, or HCO$^+$ toward our sources (e.g., Krips et al. 2011; Sakamoto et al. 2011; García-Burillo et al. 2014; Viti et al. 2014; Meier et al. 2015; Henkel et al. 2018; Tan et al. 2018; Martín et al. 2019). Weak ^{12}CN emission is detected in the spiral arms of NGC 1068 (see Fig. 2). ^{13}CN is only detected in the central regions of NGC 253, NGC 1068, and NGC 4945, and shows slightly less extended distributions than ^{12}CN (see also the end of Sect. 2.4).

3.2. ^{12}CN/^{13}CN line ratios

^{12}CN/^{13}CN line ratio maps of NGC 253, NGC 1068, and NGC 4945 are shown in Fig. 3. The line ratios are calculated using velocity-integrated intensities where the ^{13}CN lines are detected with $S/N \gtrsim 5\sigma$. The $I(^{12}\mathrm{CN})/I(^{13}\mathrm{CN})$ ratios range from 19 to 53 with an average of 30.0 ± 0.2 (errors given here and elsewhere are standard deviations of the mean) in NGC 253, from 20 to 47 with an average of 31.4 ± 0.3 in NGC 1068, and from 6 to 25 with an average of 11.5 ± 0.1 in NGC 4945. High ratios (>30) are obtained in the outskirts of the region analyzed by us in NGC 253. This shows that low ratios (<30) associate with ^{13}CN peak emission in NGC 253. Gradients are seen from the center to the northeastern and to the southwestern region of NGC 1068. Two locations in the northeast and southwest (see Table 2 and Sect. 4.2) have a low ratio (<25). For NGC 4945, low ratios (<15) associate with ^{13}CN peak emission and the northeastern region and high ratios (>15) are located in the outskirts and the southwestern region. One should note that the ^{13}CN emission is weak and shows low S/Ns on the edges of our three targets. This may lead to large uncertainties of $I(^{12}\mathrm{CN})/I(^{13}\mathrm{CN})$ ratios in these locations.

3.3. Opacities of ^{12}CN and ^{13}CN

Previous observations toward external galaxies suggest that optical depths of the ^{12}CN $N=1$–0 transition are modest (e.g., Henkel et al. 1998, 2014; Wang et al. 2009; Meier et al. 2015; König et al. 2016; Nakajima et al. 2018). This also holds for the $N=1$–0 line of the rare ^{13}CN isotopolog. Opacities can be determined by an analysis of line intensity ratios because (as already mentioned in Sect. 1) the $N=1$–0 transition is split into several spectral features. If ^{12}CN $N=1$–0 is optically thin and LTE prevails, line intensity ratios should be 2:1 for ^{12}CN (3/2–1/2)/(1/2–1/2) and 1:1.225 for ^{13}CN (3/2–1/2)/(1/2–1/2); see Fig. 1. Previous single-dish observations of ^{12}CN $N=1$–0 in galaxies indicate that the ^{12}CN (3/2–1/2)/(1/2–1/2) line intensity ratio is indeed ~2 (e.g., Henkel et al. 1998, 2014; Aladro et al. 2013, 2015; Watanabe et al. 2014; Nakajima et al. 2018).

We averaged all pixels in NGC 253, NGC 1068, and NGC 4945 for which the ^{13}CN line is detected with $S/N \gtrsim 5\sigma$. The line-integrated intensity ratios of the two ^{12}CN $N=1$–0

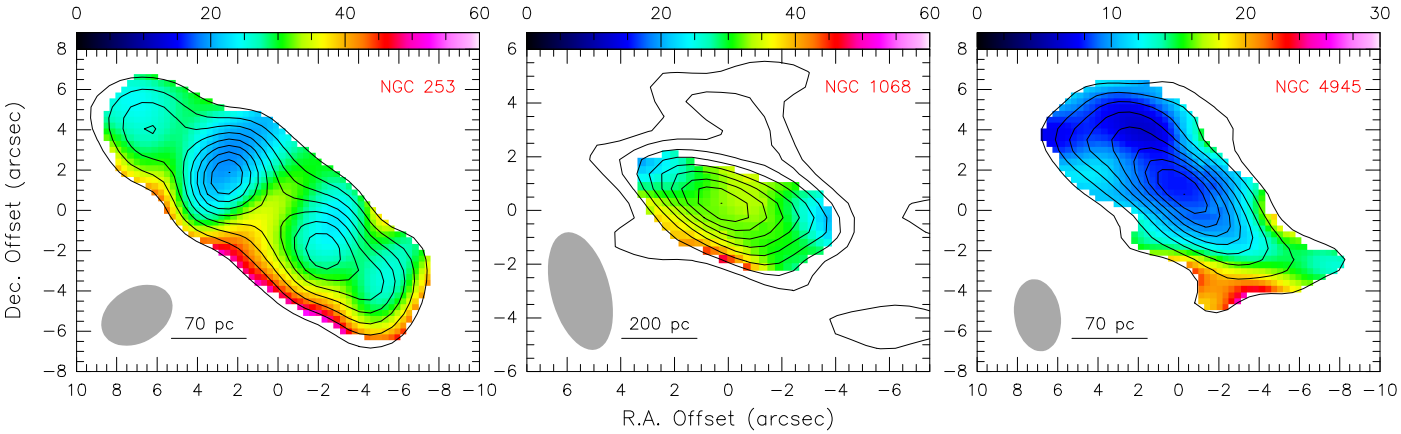

Fig. 3. Velocity-integrated intensity ratio maps of $I(^{12}\mathrm{CN})/I(^{13}\mathrm{CN})$ (see Sects. 3.2 and 3.4) in NGC 253 (*left*), NGC 1068 (*middle*), and NGC 4945 (*right*). Black contours delineate levels of ^{13}CN integrated intensity (same as in Fig. 2).

Table 2. ^{12}CN/^{13}CN line ratios, ^{12}CN opacities, and the ^{12}C/^{13}C isotope ratios toward the ^{13}CN peaks and outskirts.

Source	Offset	$I(^{12}\mathrm{CN})/I(^{13}\mathrm{CN})$	$I(^{12}\mathrm{CN}\ 3/2\text{–}1/2)/I(^{12}\mathrm{CN}\ 1/2\text{–}1/2)$	$\tau_1(^{12}\mathrm{CN}\ 3/2\text{–}1/2)$	^{12}C/^{13}C	Note
NGC 253	(6.3″, 3.9″)	26.4 ± 1.2	1.67 ± 0.03	0.79 ± 0.08	33.1 ± 3.0	Peak
	(2.7″, 1.5″)	20.0 ± 0.5	1.49 ± 0.01	1.42 ± 0.06	31.1 ± 1.6	Peak
	(–2.4″, –2.1″)	25.7 ± 1.1	1.55 ± 0.01	1.21 ± 0.05	37.2 ± 2.6	Peak
	(–4.5″, –3.6″)	27.3 ± 2.2	1.53 ± 0.02	1.28 ± 0.06	40.6 ± 4.6	Peak
	(3.9″, 5.7″)	30.3 ± 4.0	1.50 ± 0.05	1.40 ± 0.21	46.7 ± 10.6	Outskirts
	(–1.5″, –5.1″)	52.7 ± 4.4	1.66 ± 0.02	0.82 ± 0.07	66.9 ± 8.8	Outskirts
NGC 1068	(0.3″, 0.3″)	32.9 ± 2.7	1.77 ± 0.02	0.52 ± 0.05	37.3 ± 4.3	Peak
	(0.3″, –1.8″)	47.2 ± 8.0	1.63 ± 0.03	0.93 ± 0.11	62.2 ± 16.4	Outskirts
	(–0.6″, 1.2″)	35.3 ± 3.3	1.60 ± 0.09	1.03 ± 0.33	48.2 ± 13.2	Outskirts
	(3.3″, 1.8″)	20.0 ± 2.3	1.72 ± 0.05	0.66 ± 0.14	24.0 ± 4.9	Outskirts
	(–3.6″, –0.3″)	21.0 ± 3.0	1.67 ± 0.06	0.80 ± 0.18	26.5 ± 7.1	Outskirts
NGC 4945	(0.0″, 0.9″)	7.9 ± 0.3	1.78 ± 0.10	0.50 ± 0.27	9.0 ± 1.7	Peak
	(–3.0″, –4.5″)	26.6 ± 3.6	1.39 ± 0.11	1.86 ± 0.65	43.6 ± 20.8	Outskirts
	(–4.8″, –0.3″)	18.9 ± 2.2	1.39 ± 0.11	1.88 ± 0.69	34.0 ± 15.1	Outskirts

Notes. For the reference positions to the offsets given in Col. 2, see Table 1. Calibration uncertainties are not considered here but are discussed in Sect. 3.4.

features are 1.58 ± 0.11, 1.70 ± 0.02, and 1.68 ± 0.25 in NGC 253, NGC 1068, and NGC 4945, respectively, which is slightly lower than that for LTE and optically thin emission. Following the method applied by Wang et al. (2004), the optical depth of the ^{12}CN $N = 1$–0 lines can be obtained from the integrated intensity ratio of ^{12}CN (3/2–1/2)/(1/2–1/2) as

$$\frac{I(^{12}\mathrm{CN}\ J = 3/2 - 1/2)}{I(^{12}\mathrm{CN}\ J = 1/2 - 1/2)} = \frac{1 - \mathrm{e}^{-\tau_1}}{1 - \mathrm{e}^{-\tau_2}}, \quad (1)$$

where τ_1 and τ_2 are the optical depths of ^{12}CN $J = 3/2$–1/2 and 1/2–1/2, respectively, and $\tau_1 = 2\tau_2$ (see Skatrud et al. 1983 for relative LTE intensities under optically thin conditions). From the above average integrated intensity ratios of the two ^{12}CN $N = 1$–0 features the derived optical depths of ^{12}CN $J = 3/2$–1/2 are 1.1, 0.7, and 0.8 in NGC 253, NGC 1068, and NGC 4945, respectively. Opacities of ^{12}CN at ^{13}CN peaks and outskirts are also calculated in Table 2. These suggest that the opacity of ^{12}CN $N = 1$–0 slightly affects the line intensity ratios of ^{12}CN/^{13}CN in our three selected starburst galaxies. For ^{13}CN $N = 1$–0, the corresponding average line integrated intensity ratios are 1.04 ± 0.08, 1.03 ± 0.14, and 1.25 ± 0.01, which is consistent with LTE and optically thin emission considering the uncertainties of our interferometric measurements. In this work we assume that the ^{13}CN $N = 1$–0 line is optically thin in all of our three studied objects.

3.4. The ^{12}C/^{13}C isotopic ratios from CN

As mentioned in Sect. 3.3, the ^{12}CN $N = 1$–0 line is slightly influenced by saturation effects in the starburst galaxies NGC 253, NGC 1068, and NGC 4945. Therefore, in these objects the intensities of this line are not exactly proportional to CN column densities. Nevertheless, the integrated intensity ratios of ^{12}CN and ^{13}CN can be used to determine the ^{12}C/^{13}C isotope ratios. Assuming the ^{13}CN $N = 1$–0 lines are optically thin and assuming that LTE holds in NGC 253, NGC 1068, and NGC 4945 and following the method applied by Henkel et al. (2014), the ^{12}C/^{13}C isotope ratio can be obtained from the integrated intensity ratio of ^{12}CN/^{13}CN $N = 1$–0 as

$$\frac{^{12}\mathrm{C}}{^{13}\mathrm{C}} \approx \frac{f_1 \times I(^{12}\mathrm{CN}\ J = 3/2 - 1/2) + f_2 \times I(^{12}\mathrm{CN}\ J = 1/2 - 1/2)}{1.082 \times I(^{13}\mathrm{CN})}, \quad (2)$$

where $f_1 = \frac{\tau_1}{1-\mathrm{e}^{-\tau_1}}$ and $f_2 = \frac{\tau_2}{1-\mathrm{e}^{-\tau_2}}$, and τ_1 and τ_2, are the optical depths of ^{12}CN $J = 3/2$–1/2 and 1/2–1/2 (see Sect. 3.3),

Table 3. Averaged $^{12}C/^{13}C$ ratios and comparison with previous results.

Source	Range	Average	Previous result	Ref.
NGC 253	30–67	41.6 ± 0.2	40 ± 10	1, 2, 3
NGC 1068	24–62	38.3 ± 0.4	~ 40 [(a)]	4
NGC 4945	6–44	16.9 ± 0.3	40–50	1, 5, 6

Notes. [(a)]The $^{12}C/^{13}C$ ratio is derived from the uncorrected integrated intensity ratio $I(^{12}CN)/I(^{13}CN)$ taken from Nakajima et al. (2018) (see Sect. 2.4). Calibration uncertainties are not considered here but are discussed in Sect. 3.4.
References. (1) Henkel & Mauersberger (1993); (2) Henkel et al. (1993); (3) Henkel et al. (2014); (4) Nakajima et al. (2018); (5) Henkel et al. (1994b); (6) Wang et al. (2004).

respectively. The integrated intensity $I(^{13}CN)$ contains the ^{13}CN $J = 1/2$–$1/2$ and $3/2$–$1/2$ components. The factor of 1.082 is caused by the fact that a weak ^{13}CN (F_1, $F_2 = 1$–0) hyperfine feature near 108.4 GHz is both below our detection threshold and offset from the considered frequency range (see Henkel et al. 2014). The $^{12}C/^{13}C$ isotope ratios derived from the CN line ratios following Eq. (2) range from 30 to 67 with an average of 41.6 ± 0.2 in NGC 253, from 24 to 62 with an average of 38.3 ± 0.4 in NGC 1068, and from 6 to 44 with an average of 16.9 ± 0.3 in NGC 4945 (see Table 3). The uncertainty of these $^{12}C/^{13}C$ isotope ratios is ~10%, which is mainly caused by the absolute flux calibration error of ~5%.

4. Discussion

4.1. Comparison to previous $^{12}C/^{13}C$ isotopic ratio measurements

As deduced in Sect. 3.4, with ALMA we find average $^{12}C/^{13}C$ isotope ratios of 41.6 ± 0.2, 38.3 ± 0.4, and 16.9 ± 0.3 in the nuclear disks of NGC 253, NGC 1068, and NGC 4945, respectively (see Table 3). We compare our ALMA-measured $^{12}C/^{13}C$ isotope ratios with previous results obtained from single-dish observations in Table 3. For NGC 253 and NGC 1068, our average measured $^{12}C/^{13}C$ isotope ratios agree well with those obtained from the single-dish observations (Henkel & Mauersberger 1993; Henkel et al. 1993, 2014; Nakajima et al. 2018). However, our ALMA-measured $^{12}C/^{13}C$ isotope ratio is significantly lower than that obtained from the single-dish observations in NGC 4945 (Henkel & Mauersberger 1993; Henkel et al. 1994b; Wang et al. 2004). This may be caused by several factors. Previous single-dish observations may include a lot of material from outside the nuclear disk, that is, from the bar extending from galactocentric radii of 100–300 pc and from the spiral arms even farther out (see the sketch in Henkel et al. 2018). Our ALMA data cover a smaller region with galactocentric radii out to ~175 pc. The ^{12}CN distribution appears to be complex in NGC 4945 (see Sect. 3.1). The typical line widths of ^{12}CN are ~50 km s^{-1} at a velocity of ~700 km s^{-1} and ~150 km s^{-1} at a velocity of ~450 km s^{-1} in the northeastern and southwestern regions of its highly inclined ($i \sim 75°$) nuclear disk (see our Fig. 1 or Figs. 5, 11, and 13 in Henkel et al. 2018). Perhaps, the starburst is still young and the gas moving outwards through the nuclear disk is a remnant of formerly quiescent gas highly enriched in ^{13}C by AGB stars through the CNO cycle (like in our galactic center), while ^{12}C enrichment from young massive stars has not yet taken over in a substantial way.

Considering the above-mentioned uncertainties of our interferometric and previous single-dish observations in the ^{12}CN and ^{13}CN $N = 1$–0 transitions, our averaged $^{12}C/^{13}C$ isotope ratios in NGC 253 (~400 pc) and NGC 1068 (~500 pc) confirm previous results from single-dish observations. We conclude that the averaged $^{12}C/^{13}C$ isotope ratios are ~40–50 in NGC 253 and NGC 1068 and ~20–50 in NGC 4945. The apparent discrepancy between the single-dish and our interferometric results in NGC 4945 will be further discussed in Sect. 4.3. For NGC 4945 (~350 pc), our ALMA data offer a first value for the ~200 pc-sized nuclear disk, while the bar, the inner spirals, and the nuclear ~50 pc are still waiting for a dedicated measurement. Further observations combining our 12 m ALMA with 7 m ACA and Total Power (TP) data of CN and eventually also other molecules and their isotopologs could therefore provide further progress in the determination of accurate $^{12}C/^{13}C$ isotope ratios for the various distinct morphological components.

Presently, high-resolution (~3″) observations of $C^{18}O$ with ALMA toward NGC 253 suggest a low $^{12}C/^{13}C$ isotope ratio of ~21±6 (Martín et al. 2019), which is a factor of approximately two lower than our results obtained from CN. We compare our ALMA measured $^{12}CN/^{13}CN$ ratio map with their results from $^{12}C^{18}O/^{13}C^{18}O$ ratios in NGC 253 (see Fig. 3 in Martín et al. 2019). This comparison shows that the lowest $^{12}C^{18}O/^{13}C^{18}O$ ratios are associated with the northeastern hotspot which agrees with our results derived from $^{12}CN/^{13}CN$ ratios, but the distributions of $^{12}CN/^{13}CN$ and $^{12}C^{18}O/^{13}C^{18}O$ ratios are slightly different in other locations. The cause(s) of these discrepancies may be different beam sizes or different molecular distributions due to chemistry or critical densities, and could be settled by the combination of 12-m, 7-m, and TP measurements, making use of all the instruments available at the ALMA site.

4.2. Variation of the $^{12}C/^{13}C$ isotopic ratio

In our Galaxy, previous observations of H_2CO, CO, and CN indicate the presence of a $^{12}C/^{13}C$ isotope ratio gradient and further suggest a significant dispersion at a given galactocentric radius (e.g., Henkel et al. 1980, 1982, 1983, 1985, 1994a; Langer & Penzias 1990, 1993; Wilson & Rood 1994; Savage et al. 2002; Milam et al. 2005; Giannetti et al. 2014). This is expected in an inside-out formation scenario for our Galaxy and in view of radial gas streaming and potential cloud-to-cloud variations due to local supernovae or ejecta from late-type stars (e.g., Milam et al. 2005; Henkel et al. 2014). However, even in the galactic center region isotope ratios are not everywhere the same as recently discovered by Riquelme et al. (2010) and Zhang et al. (2015). The data of the former authors indicate that gas from the halo is accreted to the disk and from the outskirts of the disk to regions closer to the galactic center (Riquelme et al. 2010).

In analogy to the galactic center region, our extragalactic ALMA data also reveal spatial variations of the $^{12}C/^{13}C$ isotopic ratio within the inner ~400, ~500, and ~350 pc-sized regions of NGC 253, NGC 1068, and NGC 4945, respectively. As mentioned in Sect. 3.4, higher line ratios of $^{12}CN/^{13}CN$ indicate higher $^{12}C/^{13}C$ isotopic ratios. Therefore, the ratio maps can be used as a proxy for the relative $^{12}C/^{13}C$ isotopic ratio. $^{12}CN/^{13}CN$ line ratio maps and histograms of NGC 253, NGC 1068, and NGC 4945 are shown in Figs. 3 and 4, respectively. Variations of the $^{12}CN/^{13}CN$ line ratio as mentioned in Sect. 3.2 indicate that the highest $^{12}C/^{13}C$ isotopic ratios are located in some of the outskirts of the three starburst galaxies while the lowest ratios associate with galactic central regions and/or ^{13}CN peak emission. The velocity components in the southwest of NGC 253 and NGC 4945 (Henkel et al. 2014, 2018) suggest higher $^{12}C/^{13}C$ isotopic ratios than in the northeast. The $^{12}C/^{13}C$ isotopic ratio

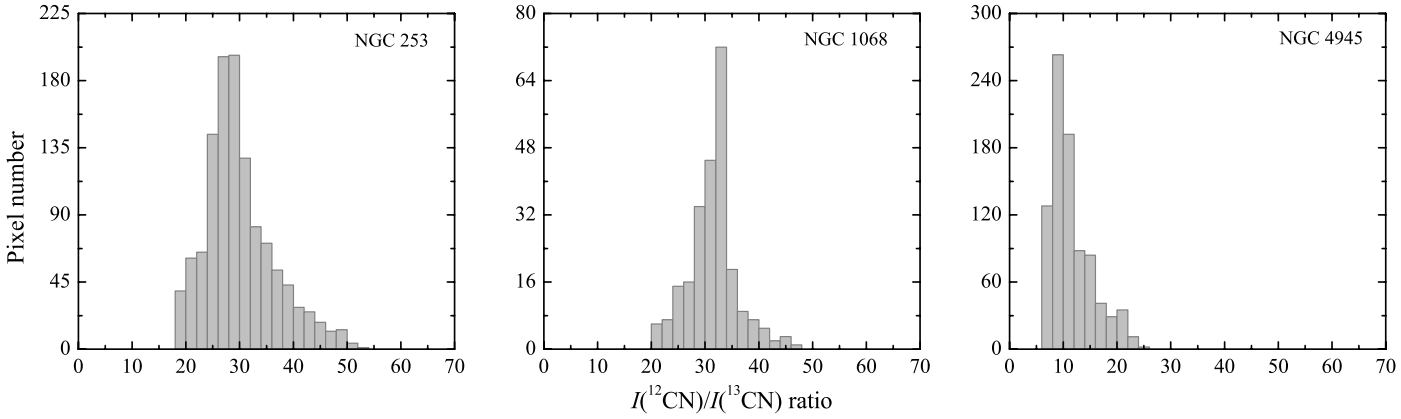

Fig. 4. Histograms showing the velocity-integrated intensity ratios of $I(^{12}CN)/I(^{13}CN)$ for NGC 253 (*left*), NGC 1068 (*middle*), and NGC 4945 (*right*).

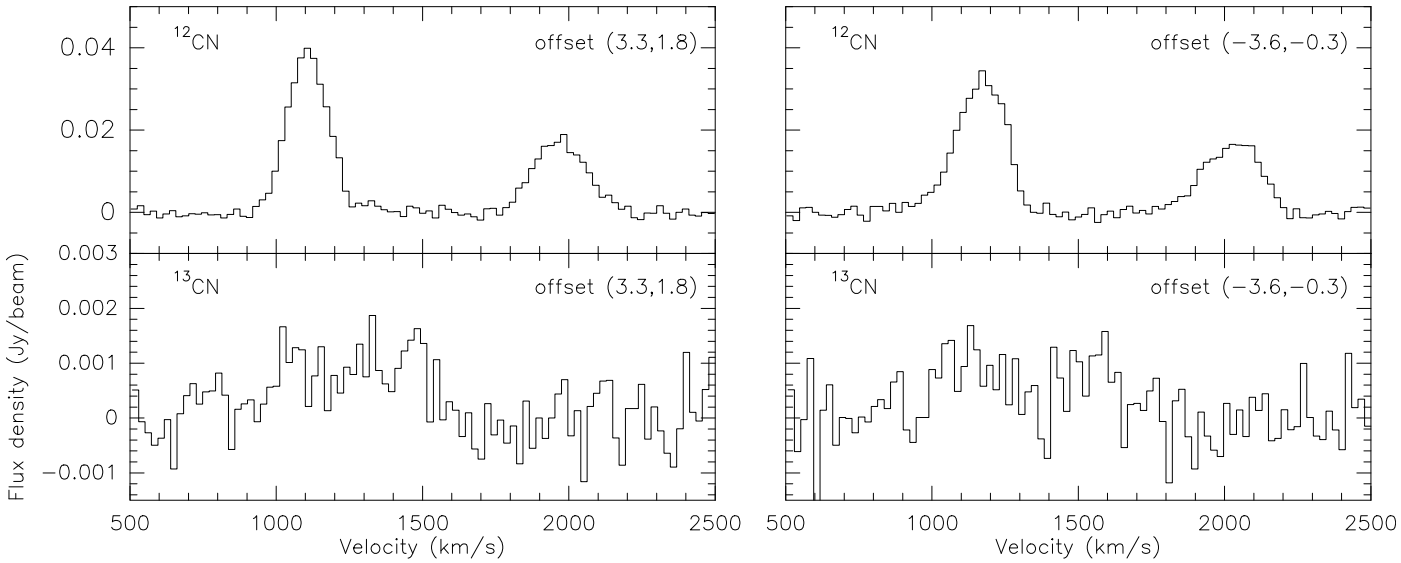

Fig. 5. ^{12}CN $N = 1$–0 (*top*) and ^{13}CN $N = 1$–0 (*bottom*) spectra toward two outflow knots OUT-III (*left*) and OUT-II (*right*) (García-Burillo et al. 2014, 2017), respectively, in NGC 1068 (see Sect. 4.2). The rest frequencies of ^{12}CN and ^{13}CN $N = 1$–0 spectra are centered at 113.491 and 108.780 GHz, respectively.

varies by factors of approximately two to three in NGC 253 and NGC 1068 and even about seven in NGC 4945 (see Fig. 4 and Table 3). While these extreme differences may in part be due to low ^{13}CN S/Ns, the differences are too large to be entirely a consequence of this effect (see Table 2).

For NGC 253, integrated intensities of ^{13}CN are highest in two hotspots, located symmetrically with respect to the nucleus, one in the northeast and the other one in the southwest. The lowest $^{12}C/^{13}C$ isotopic ratios are associated with these two hotspots (see Fig. 3) corresponding to centimeter and millimeter continuum peak emission (e.g., Turner & Ho 1985; Ulvestad & Antonucci 1997; Sakamoto et al. 2011; Krips et al. 2016; Mangum et al. 2019). The gas at these locations may be CNO-processed by intermediate-mass stars in the more distant past. Two locations with low $^{12}C/^{13}C$ isotopic ratios in the northeast (3.3″, 1.8″; offsets relative to our reference position; see Table 1) and southwest (–3.6″, –0.3″) of NGC 1068 (see Figs. 3 and 5, and Table 2) associate with two outflow knots OUT-III and II (García-Burillo et al. 2014, 2017), respectively, meaning that the highly processed gas has moved away from the center, while less processed gas may be infalling from the outer part of NGC 1068 into (at least the outer part of) the circumnuclear disk (CND) through both the halo and the bar, and the CND is dominated by the outflowing motion. The decline of the $^{12}C/^{13}C$ isotopic ratio in these locations may be influenced by the outflow from the AGN and/or by processed material near the AGN. One should note that the two outflow knots OUT-II and III are identified with ∼1″ resolution C_2H data by García-Burillo et al. (2017), which corresponds to a ∼4.5 times higher resolution (with respect to beam area) than the CN data presented here. Beam dilution effects may not be negligible. Low $^{12}C/^{13}C$ isotopic ratios in the northeast of NGC 4945 show similar values to those in the nuclear region (see Fig. 3), which indicates that it may be strongly affected by highly processed outflowing material from the nuclear region (for this, see Henkel et al. 2018) having undergone substantial star formation in the past.

4.3. The $^{12}C/^{13}C$ isotopic ratio evolution in starburst galaxies

The $^{12}C/^{13}C$ isotope ratio is a useful probe of the chemical evolution of galaxies (e.g., Milam et al. 2005; Martín et al. 2010; Henkel et al. 2014). It is believed to be a direct measure of primary to secondary nuclear processing (Wilson & Rood 1994).

The $^{12}C/^{13}C$ isotope ratio is expected to decline with time (e.g., Henkel & Mauersberger 1993; Prantzos et al. 1996; Hughes et al. 2008; Martín et al. 2010; Henkel et al. 2014; Romano et al. 2017). This leads to the very low ratios in our galactic center region. However, in case of a starburst, triggered by a bar or by a merger, gas from outside with higher ratios is flowing into the central region of a galaxy, enhancing the $^{12}C/^{13}C$ isotope ratio. A few million years after the start of a starburst, this effect will be strengthened by the ejecta from massive stars. A top-heavy stellar initial mass function could make this effect even more pronounced (e.g., Henkel & Mauersberger 1993; Romano et al. 2017; Zhang et al. 2018).

The inflow scenario discussed for starbursts may even lead to higher $^{12}C/^{13}C$ ratios for ultraluminous infrared galaxies (ULIRGs) since such objects have more powerful inflows (e.g., Toyouchi & Chiba 2015; Yabe et al. 2015; Falstad et al. 2017). Indeed, ULIRGs have not only a higher $^{12}C/^{13}C$ ratio, but are also deviating from the canonical mass-metallicity relation in the sense of having a lower metallicity for their mass or a higher mass for their metallicity (Pereira-Santaella et al. 2017). More moderate starburst galaxies have experienced less inflow, which may suggest lower $^{12}C/^{13}C$ isotope ratios. In comparison, our Galaxy shows only weak signs of inflow (e.g., Morris & Serabyn 1996; Riquelme et al. 2010), which is reflected in the lower $^{12}C/^{13}C$ isotope ratios measured in its central molecular zone. The CN data presented here indicate that the averaged $^{12}C/^{13}C$ isotope ratios in the nuclear regions of NGC 253 and NGC 1068 are higher than in our galactic center region. Nevertheless, the averaged $^{12}C/^{13}C$ isotope ratios in our selected nearby starburst galaxies are lower than previous observational results in the well-studied ULIRGs Arp 220 and Mrk 231 (∼100; González-Alfonso et al. 2012; Henkel et al. 2014), and also in the high-z Cloverleaf ULIRG/QSO (≳100; Henkel et al. 2010). This confirms the trend of declining $^{12}C/^{13}C$ values with time and metallicity proposed by Henkel et al. (2014).

Measurements of the $^{12}C/^{13}C$ isotope ratio based on CN lines have the potential to reveal the degree of gas processing in the nuclear regions of starburst galaxies. More galaxies are needed to study nucleosynthesis, to constrain galaxy dynamics, and to discriminate between different evolutionary stages to more closely follow the secular decline of $^{12}C/^{13}C$ ratios that is occasionally interrupted by inflow and starburst activity. With ALMA it is possible to extend such studies to objects at greater distances.

5. Summary

We measured the $^{12}C/^{13}C$ isotopic ratio in the nuclear regions of three nearby starburst galaxies NGC 253, NGC 1068, and NGC 4945 making use of the ^{12}CN and ^{13}CN $N = 1$–0 lines in the ALMA Band 3 at frequencies near 110 GHz. The main results can be summarized as follows.

1. The $^{12}C/^{13}C$ isotopic ratios derived from the ^{12}CN and ^{13}CN line ratios range from 30 to 67 with an average of 41.6 ± 0.2 in NGC 253, from 24 to 62 with an average of 38.3 ± 0.4 in NGC 1068, and from 6 to 44 with an average of 16.9 ± 0.3 in NGC 4945. The $^{12}C/^{13}C$ isotopic ratios vary by factors of approximately two to three in NGC 253 (∼400 pc) and NGC 1068 (∼500 pc) and about seven in NGC 4945 (∼350 pc). The large scatter of values, particularly in NGC 4945, is certainly in part a consequence of the limited sensitivity of our data. Nevertheless, the variations are too large to be only caused by this effect, suggesting the presence of real variations, as recently found in our galactic center region.
2. The highest $^{12}C/^{13}C$ isotopic ratios are located in the outskirts of the nuclear regions of the three starburst galaxies. The lowest ratios are associated with the northeastern and southwestern molecular peaks of NGC 253, the northeastern and southwestern edge of the mapped region in NGC 1068, and the very center of NGC 4945.
3. The measured $^{12}C/^{13}C$ isotopic ratios in NGC 1068 indicate that the highly processed gas has moved away from the center and less processed gas may be infalling from the outer part of NGC 1068 into the CND through both the halo and the bar.
4. Low $^{12}C/^{13}C$ isotopic ratios in the central regions of these starburst galaxies indicate the presence of highly processed material.
5. Our results agree with the scenario of $^{12}C/^{13}C$ ratios slowly decreasing in galaxies with time.

Acknowledgements. The authors thank the anonymous referee for helpful comments. This work acknowledges support by The Heaven Lake Hundred-Talent Program of Xinjiang Uygur Autonomous Region of China, The National Natural Science Foundation of China under grant 11433008, and The Collaborative Research Council 956, subproject A6, funded by the Deutsche Forschungsgemeinschaft (DFG). C. H. acknowledges support by Chinese Academy of Sciences President's International Fellowship Initiative under Grant No. 2019VMA0039. Y. G. was supported by the National key R&D program under grant 2017YFA0402702. This paper makes use of the following ALMA data: ADS/JAO.ALMA#2011.0.00172.S and 2013.1.01151.S. ALMA is a partnership of ESO (representing its member states), NSF (USA) and NINS (Japan), together with NRC (Canada), NSC and ASIAA (Taiwan), and KASI (Republic of Korea), in cooperation with the Republic of Chile. The Joint ALMA Observatory is operated by ESO, AUI/NRAO and NAOJ. This research has made use of the NASA/IPAC Extragalactic Database (NED) which is operated by the Jet Propulsion Laboratory, California Institute of Technology, under contract with the National Aeronautics and Space Administration. This research has used NASA's Astrophysical Data System (ADS).

References

Aalto, S., Polatidis, A. G., Hüttemeister, S., et al. 2002, A&A, 381, 783
Aalto, S., Monje, R., & Martín, S. 2007, A&A, 475, 479
Aladro, R., Viti, S., Bayet, E., et al. 2013, A&A, 549, A39
Aladro, R., Martín, S., Riquelme, D., et al. 2015, A&A, 579, A101
Adande, G. R., & Ziurys, L. M. 2012, ApJ, 744, 194
Bachiller, R., Fuente, A., Bujarrabal, V., et al. 1997, A&A, 319, 235
Bland-Hawthorn, J., Gallimore, J. F., Tacconi, L. J., et al. 1997, Ap&SS, 248, 9
Chiappini, C., Matteucci, F., & Romano, D. 2001, ApJ, 554, 1044
Chou, R. C. Y., Peck, A. B., Lim, J., et al. 2007, ApJ, 670, 116
Chung, A., Yun, M. S., Naraynan, G., et al. 2011, ApJ, 732, 15
Curran, S. J., Johansson, L. E. B., Bergman, P., et al. 2001, A&A, 367, 457
Dahlem, M., Golla, G., Whiteoak, J. B., et al. 1993, A&A, 270, 29
Davis, T. A. 2014, MNRAS, 445, 2378
Falstad, N., González-Alfonso, E., Aalto, S., & Fischer, J. 2017, A&A, 597, A105
Fuente, A., García-Burillo, S., Gerin, M., et al. 2005, ApJ, 619, 155
Gao, Y., & Solomon, P. M. 2004, ApJS, 152, 63
Gallimore, J. F., Baum, S. A., O'Dea, C. P., et al. 1996, ApJ, 462, 740
Gallimore, J. F., Baum, S. A., & O'Dea, C. P. 1997, Nature, 388, 852
Gallimore, J. F., Henkel, C., Baum, S. A., et al. 2001, ApJ, 556, 694
García-Burillo, S., Usero, A., Fuente, A., et al. 2010, A&A, 519, A2
García-Burillo, S., Combes, F., Usero, A., et al. 2014, A&A, 567, A125
García-Burillo, S., Combes, F., Ramos Almeida, C., et al. 2016, ApJ, 823, 12
García-Burillo, S., Viti, S., Combes, F., et al. 2017, A&A, 608, A56
Giannetti, A., Wyrowski, F., Brand, J., et al. 2014, A&A, 570, A65
Ginard, D., Fuente, A., García-Burillo, S., et al. 2015, A&A, 578, A49
González-Alfonso, E., Fischer, J., Graciá-Carpio, J., et al. 2012, A&A, 541, A4
Gratier, P., Bron, E., Gerin, M., et al. 2017, A&A, 599, A100
Green, C. E., Cunningham, M. R., Green, J. A., et al. 2016, MNRAS, 457, 2470
Greenhill, L. J., Gwinn, C. R., Antonucci, R., et al. 1996, ApJ, 472, 21
Greenhill, L. J., Moran, J. M., & Herrnstein, J. R. 1997, ApJ, 481, 23
Güsten, R., Henkel, C., & Batrla, W. 1985, A&A, 149, 195

Han, X. H., Zhou, J. J., Wang, J. Z., et al. 2015, A&A, 576, A131
Henkel, C., & Mauersberger, R. 1993, A&A, 274, 730
Henkel, C., Walmsley, C. M., & Wilson, T. L. 1980, A&A, 82, 41
Henkel, C., Wilson, T. L., & Bieging, J. 1982, A&A, 109, 344
Henkel, C., Wilson, T. L., Walmsley, C. M., & Pauls, T. 1983, A&A, 127, 388
Henkel, C., Güsten, R., & Gardner, F. F. 1985, A&A, 143, 148
Henkel, C., Mauersberger, R., & Schilke, P. 1988, A&A, 201, 23
Henkel, C., Whiteoak, J. B., Nyman, L. A., & Harju, J. 1990, A&A, 230, 5
Henkel, C., Baan, W. A., & Mauersberger, R. 1991, A&ARv, 3, 47
Henkel, C., Mauersberger, R., Wiklind, T., et al. 1993, A&A, 268, 17
Henkel, C., Wilson, T. L., Langer, N., et al. 1994a, LNP, 439, 72
Henkel, C., Whiteoak, J. B., & Mauersberger, R. 1994b, A&A, 284, 17
Henkel, C., Chin, Y. N., Mauersberger, R., et al. 1998, A&A, 329, 443
Henkel, C., Tarchi, A., Menten, K. M., & Peck, A. B. 2004, A&A, 414, 117
Henkel, C., Downes, D., Weiß, A., et al. 2010, A&A, 516, A111
Henkel, C., Asiri, H., Ao, Y., et al. 2014, A&A, 565, A3
Henkel, C., Mühle, S., Bendo, G., et al. 2018, A&A, 615, A155
Hily-Blant, P., Walmsley, M., Pineau Des Forêts, G., et al. 2008, A&A, 480, 5
Hitschfeld, M., Aravena, M., Kramer, C., et al. 2008, A&A, 479, 75
Hodge, P. 1989, ARA&A, 27, 139
Hughes, G. L., Gibson, B. K., Carigi, L., et al. 2008, MNRAS, 390, 1710
Jiang, X., Wang, J., & Gu, Q. 2011, MNRAS, 418, 1753
Jiménez-Donaire, M. J., Bigiel, F., Leroy, A. K., et al. 2017, MNRAS, 466, 49
Karachentsev, I. D., Tully, R. B., Dolphin, A., et al. 2007, AJ, 133, 504
König, S., Aalto, S., Muller, S., et al. 2016, A&A, 594, A70
Krips, M., Martín, S., Eckart, A., et al. 2011, ApJ, 736, 37
Krips, M., Martín, S., Peck, A. B., et al. 2016, ApJ, 821, 112
Langer, W. D., & Penzias, A. A. 1990, ApJ, 357, 477
Langer, W. D., & Penzias, A. A. 1993, ApJ, 408, 539
Langer, W. D., Graedel, T. E., Frerking, M. A., et al. 1984, ApJ, 277, 581
Mangum, J. G., Ginsburg, A. G., Henkel, C., et al. 2019, ApJ, 871, 170
Marconi, A., Oliva, E., van der Werf, P. P., et al. 2000, A&A, 357, 24
Martín, S., Mauersberger, R., Martín-Pintado, J., et al. 2006, ApJS, 164, 450
Martín, S., Aladro, R., Martín-Pintado, J., et al. 2010, A&A, 522, A62
Martín, S., Krips, M., Martín-Pintado, J., et al. 2011, A&A, 527, A36
Martín, S., Muller, S., Henkel, C., et al. 2019, A&A, 624, A125
Mauersberger, R., Henkel, C., Whiteoak, J. B., et al. 1996, A&A, 309, 705
McCarthy, T. P., Ellingsen, S. P., Breen, S. L., et al. 2018, MNRAS, 480, 4578
McMullin, J. P., Waters, B., Schiebel, D., et al. 2007, ASP Conf. Ser., 376, 127
Meier, D. S., Turner, J. L., & Beck, S. C. 2014, ApJ, 795, 107
Meier, D. S., Walter, F., Bolatto, A. D., et al. 2015, ApJ, 801, 63
Milam, S. N., Savage, C., Brewster, M. A., et al. 2005, ApJ, 634, 1126
Milam, S. N., Woolf, N. J., & Ziurys, L. M. 2009, ApJ, 690, 837
Morris, M., & Serabyn, E. 1996, ARA&A, 34, 645
Mouhcine, M., Ferguson, H. C., Rich, R. M., et al. 2005, ApJ, 633, 810
Mould, J., & Sakai, S. 2008, ApJ, 686, 75
Nakajima, T., Takano, S., Kohno, K., et al. 2015, PASJ, 67, 8
Nakajima, T., Takano, S., Kohno, K., et al. 2018, PASJ, 70, 7
Nguyen, Q. R., Jackson, J. M., Henkel, C., et al. 1992, ApJ, 399, 521
Pence, W. D. 1981, ApJ, 247, 473
Pereira-Santaella, M., Rigopoulou, D., Farrah, D., Lebouteiller, V., & Li, J. 2017, MNRAS, 470, 1218
Pérez-Beaupuits, J. P., Aalto, S., & Gerebro, H. 2007, A&A, 476, 177
Pérez-Beaupuits, J. P., Spaans, M., van der Tak, F. F. S., et al. 2009, A&A, 503, 459
Prantzos, N., Aubert, O., & Audouze, J. 1996, A&A, 309, 760
Puche, D., Carignan, C., & van Gorkom, J. 1991, AJ, 101, 456
Qiu, J., Wang, J., Shi, Y., Zhang, J., Fang, M., & Li, F. 2018, A&A, 613, A3
Rekola, R., Richer, M. G., McCall, M. L., et al. 2005, MNRAS, 361, 330
Riquelme, D., Amo-Baladrón, M. A., Martín-Pintado, J., et al. 2010, A&A, 523, A51
Romano, D., Matteucci, F., Zhang, Z. Y., et al. 2017, MNRAS, 470, 401
Rodríguez-Franco, A., Martín-Pintado, J., & Fuente, A. 1998, A&A, 329, 1097
Roueff, E., Loison, J. C., & Hickson, K. M. 2015, A&A, 576, A99
Saito, T., Iono, D., Yun, M. S., et al. 2015, ApJ, 803, 60
Sakamoto, K., Mao, R. Q., Matsushita, S., et al. 2011, ApJ, 735, 19
Sakamoto, K., Aalto, S., Combes, F., Evans, A., & Peck, A. 2014, ApJ, 797, 90
Savage, C., Apponi, A. J., Ziurys, L. M., & Wyckoff, S. 2002, ApJ, 578, 211
Schinnerer, E., Eckart, A., Tacconi, L. J., et al. 2000, ApJ, 533, 850
Skatrud, D. D., De Lucia, F. C., Blake, G. A., et al. 1983, J. Mol. Spectr., 99, 35
Tan, Q. H., Gao, Y., Zhang, Z. Y., et al. 2018, ApJ, 860, 165
Toyouchi, D., & Chiba, M. 2015, ApJ, 810, 18
Turner, J. L., & Ho, P. T. P. 1985, ApJ, 299, 77
Ulvestad, J. S., & Antonucci, R. R. J. 1997, ApJ, 488, 621
Usero, A., García-Burillo, S., Fuente, A., et al. 2004, A&A, 419, 897
Viti, S., García-Burillo, S., Fuente, A., et al. 2014, A&A, 570, A28
Wang, J., Zhang, Z. Y., Qiu, J., Shi, Y., Zhang, J., & Fang, M. 2014, ApJ, 796, 57
Wang, M., Henkel, C., Chin, Y. N., et al. 2004, A&A, 422, 883
Wang, M., Chin, Y.-N., Henkel, C., et al. 2009, ApJ, 690, 580
Watanabe, Y., Sakai, N., Sorai, K., & Yamamoto, S. 2014, ApJ, 788, 4
Watanabe, Y., Nishimura, Y., Harada, N., et al. 2017, ApJ, 845, 116
Wild, W., Harris, A. I., Eckart, A., et al. 1992, A&A, 265, 447
Wilson, C. D. 2018, MNRAS, 477, 2926
Wilson, T. L. 1999, Rep. Prog. Phys., 62, 143
Wilson, T. L., & Rood, R. 1994, ARA&A, 32, 191
Wouterloot, J. G. A., & Brand, J. 1996, A&AS, 119, 439
Wouterloot, J. G. A., Henkel, C., Brand, J., & Davis, G. R. 2008, A&A, 487, 237
Yabe, K., Ohta, K., Akiyama, M., et al. 2015, ApJ, 798, 45
Yamagishi, M., Nishimura, A., Fujita, S., et al. 2018, ApJS, 235, 9
Yan, Y. T., Zhang, J. S., Henkel, C., et al. 2019, ApJ, 877, 154
Yaqoob, T. 2012, MNRAS, 423, 3360
Zhang, J. S., Sun, L. L., Riquelme, D., et al. 2015, ApJS, 219, 28
Zhang, Z. Y., Romano, D., Ivison, R. J., et al. 2018, Nature, 558, 260